Inviscid Transonic Flow over Airfoils

R. MAGNUS* AND H. YOSHIHARA†
Convair Division of General Dynamics, San Diego, Calif.

A procedure is presented to calculate steady supercritical planar flows over lifting airfoils using an unsteady approach, where the steady flow is obtained as the asymptotic flow for large times. The unsteady flow is generated by impulsively imposing the airfoil boundary condition in an initially uniform flow. The resulting flow is calculated by a finite difference analogue to the unsteady Euler equations using a diffusing second-order difference scheme. Here an artificial viscosity appears by which shock waves acquire a steep profile. The procedure is used to calculate the flows over one of the nonlifting symmetrical shockless profiles derived by Nieuwland, using the hodograph method, and over a lifting NACA 64A-410 profile. Results agree well with experiments, with local differences accountable by a Busemann-Guderley instability in the first case, and by viscous effects in the second case.

I Introduction

WE shall be concerned here with planar steady flows over lifting airfoils at high subsonic supercritical Mach numbers. We shall restrict ourselves to inviscid flows. It is well known, however, that in some cases viscous effects play a significant role, so that the present effort must in these cases be considered only as an element of the over-all problem, which must treat the inviscid flow and the boundary-layer flow in a coupled fashion. In many cases, however, viscous effects play only a perturbing role, so that an inviscid result would directly lead to a physically meaningful result.

The calculation of the inviscid supercritical flow over a prescribed airfoil must be carried out by a numerical method, since the problem is essentially nonlinear. The coexistence of regions of subsonic and supersonic flows, with their highly differing characters, as well as the possible appearance of shock waves at locations unknown beforehand, makes a direct numerical attack on the problem in the steady state extremely difficult. If, however, one considers the problem to be unsteady, then the problem mathematically is significantly simplified, since in the unsteady representation the flow equations become hyperbolic in contrast to the mixed elliptic-hyperbolic character in the steady representation. With suitable initial and boundary conditions, the desired steady solution may then be obtained as the asymptotic flow for large times. If additionally an artificial viscosity is introduced indirectly in the numerical procedure by the use of a diffusing difference scheme or by an appropriate second-order differencing scheme, the difficulty of fitting a discontinuous shock wave into the flow is circumvented, since with the artificial viscosity the approximate numerical representation of the flow becomes entirely continuous. Shock waves, instead of being discontinuous, will acquire a profile and will appear automatically as narrow zones where the flow variables acquire a steep gradient. Moreover, the thickness of the shock waves may be made in principle arbitrarily small by taking a limit of vanishing artificial viscosity through the use of a smaller mesh; and the corresponding finite difference solution will approach the exact inviscid solution in this limit.[1]

We may, by the aforementioned process, eliminate the difficulties mentioned previously, but at the inconvenience of having to introduce a third independent variable; namely, the time. In the present considerations we have simply taken the unsteady, compressible, Euler equations, which as mentioned previously are a hyperbolic system of equations. The sequence of flows generated at succeeding times represent physically realistic flows, provided the initial state is realistic. If we are interested, however, only in the steady flow at large times, then of course the intervening unsteady flows per se would be of no interest, except that they may serve as a qualitative guide to the correct evolution of the steady flow. In this case an intriguing possibility arises of introducing to the steady Euler equations other time derivatives, other than the physically correct unsteady Euler terms to obtain a set of equations, whose solutions may subside more speedily to the steady state. Such terms should lead, in the case of a hyperbolic system, to a system of Monge (characteristic) cones which everywhere approach right-circular cones. The desirability of this choice will be evident when one recalls that in a numerical method the allowable time step is dictated by the Courant-Friedrichs-Lewy condition (CFL condition) by the steepest inclination of the Monge cone; whereas the lateral propagation of the flow adjusting waves will be restricted to the interior of the cone. In the case of the unsteady Euler equations, the slowness of the convergence to the steady state can be accounted for in large part by the inclination of the Monge cone axis, with respect to the time-axis leading to a slow upwind propagation of the flow adjusting waves. Clearly, a reduction to a parabolic system (with a Monge cone angle of 90°) would fulfill our requirements. It must be remembered that in this case, when a finite difference method is used, the parabolic character is lost, with the truncation error reverting the character of the equation back to a hyperbolic system where the Monge cone is framed by suitable diagonals of the lattice system.

Obviously, the aforementioned possibilities are promising and will be subjected to future inquiry. But for the present paper we shall apply a finite difference approximation to the exact, unsteady Euler equations, using a modification of the explicit Lax-Wendroff second-order differencing scheme. The resulting system of difference equations will then be used to study the sequence of unsteady flows generated when an initially uniform flow is impulsively disturbed by the abrupt imposition of the boundary condition at the profile. The procedure will then be applied to two cases. The first case is of special significance and is one of the nonlifting, symmetric, shockless profiles derived by Nieuwland,[2] using the hodograph method. As is well known, shockless flows, however they are derived, have been shown to be unstable,[3–5] such that an infinitesimal perturbation of the freestream or of the supersonic portion of the profile leads to a flow that is no longer shockless. The impulsive manner in which we

Presented as Paper 70-47 at the AIAA 8th Aerospace Sciences Meeting, New York, January 19–21, 1970; submitted February 16, 1970; revision received June 24, 1970. Study sponsored by the Air Force Flight Dynamics Laboratory Contract F33615-69-C-1180 under L. Keel.

* Senior Staff Scientist, Engineering Technologies Directorate.
† Engineering Staff Specialist, Engineering Technologies Directorate. Associate Fellow AIAA.

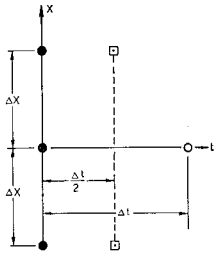

Fig. 1 Lattice configuration for modified Lax-Wendroff scheme.

initiate the flow will furnish adequate perturbing influences to establish the stability of such shockless flows; at the same time a calculation will reveal the consequence of the instability, if the flow is unstable. To be sure, no numerical calculation will ever serve to prove or disprove an analytical result, but within limits, an indication of the sensitivity of the flow to such an instability or more practically, the strength of the resulting shocks, if they do occur, may be obtained from such a numerical result. It also must be strongly emphasized that the appearance of even the weakest of shocks, those which may not even be resolvable in a refined numerical calculation or in a carefully diagnosed wind-tunnel test, will serve to corroborate the previously mentioned nonexistence theories. If the resulting shocks arising from the instability are sufficiently weak, then quite clearly shockless profiles, despite the instability, will still be highly desirable.

For the remaining example we shall calculate the flow over a NACA 64A-410 profile at 4° angle of attack at a freestream Mach number of 0.72. This example will illustrate the procedure for a lifting case where a shock of significant strength is present.

In the next sections we shall first formulate the unsteady problem, describe the difference analogues, and finally give the results for the examples, comparing them with existing experimental results.

II Unsteady Initial Boundary-Value Problem

In the following, we shall use the usual notation for the flow variables. In conservation form the unsteady Euler equations in a Cartesian coordinate system are given by the vector equation

$$\frac{\partial}{\partial t}\begin{Bmatrix}\rho\\ \rho u\\ \rho v\end{Bmatrix} = -\frac{\partial}{\partial x}\begin{Bmatrix}\rho u\\ \rho u^2 + p\\ \rho uv\end{Bmatrix} - \frac{\partial}{\partial y}\begin{Bmatrix}\rho v\\ \rho uv\\ \rho v^2 + p\end{Bmatrix} \tag{1}$$

Departure from an isentropic and irrotational flow results from the appearance of curved shock waves, but the strength of any expected shocks are sufficiently weak for cases of interest to us so that we may assume an isentropic flow. Therefore, we have

$$(p/p_\infty)/(\rho/\rho_\infty)^\gamma = \exp[(s - s_\infty)/C_v] \sim 1 \tag{2}$$

where s is the entropy, and the subscript ∞ denotes the freestream conditions. Using Eq. (2) to eliminate p from Eq. (1), results in a hyperbolic system of three equations for the dependent variables u, v, and ρ.

For the boundary conditions far from the body, we shall require the flow to approach a uniform flow with the conditions $u = u_\infty$, $v = 0$, and $\rho = \rho_\infty$. For all positive times, we shall require the component of the velocity vector normal to the profile to be zero and the Kutta condition to be fulfilled at the sharp trailing edge. Initially, we assume that the profile is sufficiently leaky, so that a uniform flow at the freestream condition persists everywhere. At zero time we impulsively turn off the leakiness by imposing suddenly the zero normal velocity and Kutta conditions. Equation (1) will then be used to determine the subsequent subsidence of the flow to the desired steady state.

III Finite Difference Analogue

The system of partial differential equations given by Eq. (1) is now replaced by a system of difference equations, by first replacing the continuous x, y, and t space by a lattice of nodal points, and then substituting the partial derivatives by partial differences expressed in terms of the values of the dependent variables at the lattice points. For our case, we shall use a rectangular lattice with the spacing Δx, Δy, and Δt in the respective coordinate directions. For the partial derivatives, we shall adopt a modification of the explicit Lax-Wendroff second-order differencing scheme, which may be illustrated in principle by applying it to the simple equation

$$\partial u/\partial t = \partial u/\partial x \tag{3}$$

Consider now the basic lattice element as shown in Fig. 1; and in particular consider the marching procedure of determining the value of u_0^1 when knowing the values u_0^0, u_1^0, and u_{-1}^0 at the initial time plane; here we have used the notation $u(m\Delta x, n\Delta t) = u_m^n$.

The differencing scheme is now to be carried out in two steps. In the first step we shall determine $u_1^{1/2}$ and $u_{-1}^{1/2}$ on an auxiliary time plane at $t = \Delta t/2$, by means of the equations

$$\begin{aligned} u_1^{1/2} &= u_1^0 + \frac{\Delta t}{2}\left(\frac{3u_1^0 - 4u_0^0 + u_{-1}^0}{2\Delta x}\right)\\ u_{-1}^{1/2} &= u_{-1}^0 + \frac{\Delta t}{2}\left(\frac{-u_1^0 + 4u_0^0 - 3u_{-1}^0}{2\Delta x}\right)\end{aligned} \tag{4}$$

Here the quantities in the parentheses are the finite difference expressions for $\partial u/\partial x$, which from Eq. (3) is equal to $\partial u/\partial t$.

Eqs. (4), therefore represent linear Taylor expansions. The second and final step gives the sought value u_0^1 in terms of the known initial values by the Taylor expansion

$$u_0^1 = \left[(1 - k)u_0^0 + k\left(\frac{u_1^0 + u_{-1}^0}{2}\right)\right] + \Delta t\left(\frac{u_1^{1/2} - u_{-1}^{1/2}}{2\Delta x}\right) \tag{5}$$

where the values of $u_1^{1/2}$ and $u_{-1}^{1/2}$ are given by Eq. (4), and k is a constant such that $0 \leq k \leq 1$. Note here that the linear Taylor coefficient is evaluated on the auxiliary time plane at $\frac{1}{2}\Delta t$. In the term in the square brackets of Eq. (5), use is made of the equivalence of u_0^0 with the average of u_1^0 and u_{-1}^0. The bracketed term thus represents a weighted average of these two equivalents with the weighting constant k. The constant k is called the diffusive damping coefficient, and the appropriateness of this name will be more evident shortly. When the coefficient k is zero or is of order Δx, the procedure just mentioned leads to an approximation with a truncation error of the order of Δt^3 or Δx^3, otherwise the errors will be of second order.

Again, using the simplified Eq. (3), the significance of the diffusive damping constant k, and the generation of an artificial viscosity by the use of the aforementioned second-order difference scheme can both be shown by now considering the resulting difference equation, assuming that the various terms in this equation are continuous functions of their arguments; and then expanding each of the terms in a Taylor series terminating each series consistently after the linear term.[6] The result will be a differential equation "equivalent" to the difference equation containing the original differential Eq. (3) with however, two additional terms, both representing a diffusion effect. One of the diffusion terms contains a space derivative of second order with a coefficient of viscosity proportional to k; whereas the second term contains a third derivative with a coefficient of viscosity proportional to Δt. The latter viscosity arises from the use of the second-order differencing scheme; and its similarity to the artificial viscosity of Von Neumann and Richtmyer led Lax to label it also as an artificial viscosity. The preceeding diffusive terms also, clearly, represent the truncation error which arises due to the use of the difference scheme. The

equivalent differential equation as previously derived is especially useful, since it provides an insight into the numerical process. One sees clearly, for example, from the equivalent differential equation that the undesirable truncation error terms are in fact responsible for the indispensable damping necessary for stability.‡ In a calculation, an examination of the diffusive terms would also identify local flow regions where nonlinear instabilities would be expected by noting where these terms vanished.

The preceding procedure differs from the Lax-Wendroff procedure in two aspects; the first is the introduction of the diffusive damping coefficient k($k = 0$ in the Lax-Wendroff procedure); and the second is in the positioning of the points on the auxiliary time plane at $\pm\Delta x$, instead of at $\pm\frac{1}{2}\Delta x$. The latter modification has the convenience of not having to introduce points at the half-mesh locations in the space plane. The former modification for nonzero values of k has an essential advantage of enhancing the artificial viscosity beyond that arising by the use of the second-order scheme when such additional damping is required locally to maintain stability. This flexibility, however, is possibly obtained at the expense of a decreased order of accuracy, depending on the relative magnitude of k.

In the previous paragraphs we have illustrated the finite difference analogue for the case of the simplified Eq. (3). Let us next examine the added complications if we apply the same procedure instead to the unsteady Euler equation given by Eq. (1). Here all of the considerations arising for the simplified equation would apply with, however, an additional complexity arising as a result of the presence of the additional partial derivatives in y, as well as coefficients for the space derivatives which are, in general, functions of u, v, and ρ. To retain the second-order accuracy, these latter coefficients must be evaluated consistently; that is, at appropriate points in the initial time plane when applying the first step in Eq. (4), and in the auxiliary time plane (at $t = \frac{1}{2}\Delta t$) when applying the second step in Eq. (5). The addition of the y derivatives causes no essential difficulties.

Use of the preceding procedure enables one to march in time for interior points where all of the points involved lie within the flow domain. For lattice points at or near the boundaries, where the regular configuration is no longer possible, we must modify the procedure. Moreover, at the boundaries, we must introduce a method to impose the boundary conditions. The procedure can be significantly simplified if the lattice could be continued in a regular manner into the interior of the profile. However the analytical continuation of the flow into the profile interior, primarily in the nose region, contains severe gradients in the flow variables and is frequently inflicted with singularities in the form of limiting lines (or regression lines), when the flow is supersonic. With such a severe flow in the interior of the profile, it would be imprudent to extend the lattice into this region.

Thus, to calculate the points in the vicinity of and on the profile we superimpose on the underlying basic rectangular network of points a sequence of rotated nine-point lattice elements, one of which is shown in Fig. 2.§ The superimposed lattice elements are identical to the underlying basic elements, but are rotated such that the bottom triplet of points forms a tangent to the airfoil surface at the middle point. Each rotated lattice element is used to advance the solution at the center point as well as the boundary point. For the latter point, a suitable asymmetric difference scheme is used. Sufficient overlap of this rotated sequence of lattice

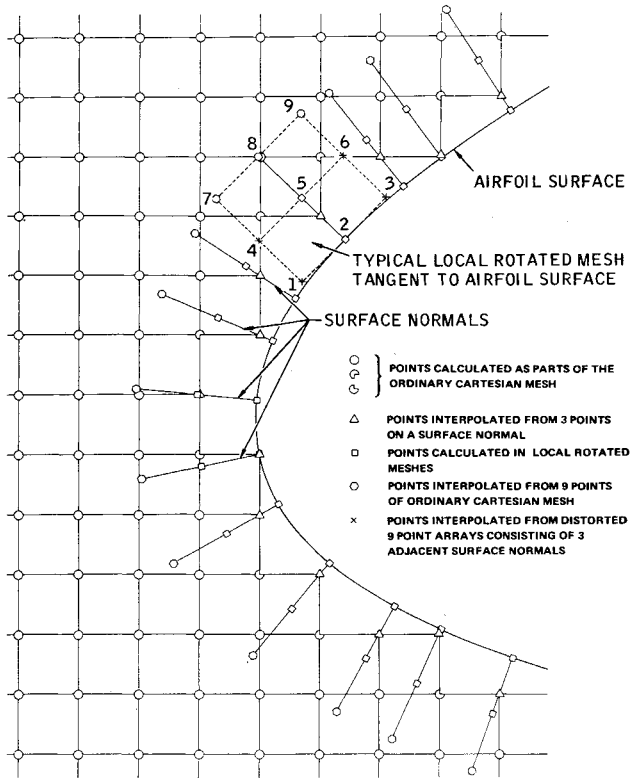

Fig. 2 Mesh system used for calculation of field in the vicinity of the airfoil.

elements, with the underlying regular network, is maintained to obtain the necessary continuity between the two systems of lattice points. To illustrate the calculational technique for points near the airfoil, let us in particular carry out the marching process to obtain the solution at Pt. 2 of Fig. 2. At the same time, the procedure to fulfill the boundary condition at the airfoil will be illustrated. The problem is now to determine the solution at Pt. 2 at the time $t = \Delta t$, knowing the initial values at $t = 0$, at the nine points of the rotated lattice element, which at the same time fulfills the boundary condition. The required initial values at the nine points of the rotated lattice element are obtained from the calculations at a prior time step, by a suitable interpolation of the results from the basic as well as the rotated lattice elements. The first step is now to introduce an asymmetric difference scheme to determine u, v, and ρ at Pt. 2 at $t = \Delta t$. The resulting velocity normal to the airfoil is not zero. We then impulsively introduce a plane unsteady wave at Pt. 2 tangent to the airfoil at Pt. 2 of an appropriate strength and velocity, which reduces the normal velocity to zero. This plane-unsteady wave is simply an artifice to introduce the influence of those points in the interior of the profile that fall in the domain of dependence of the boundary point in question. The velocity component tangent to the surface is kept invariant. The necessary wave strength, its velocity as well as the density behind the wave, are obtained by the jump conditions for a moving wave.

For the fulfillment of the conditions at infinity, we first represent the far field by a polar coordinate system; and then map the region exterior to a circle of a given large radius into the interior of a circle by an inverse transformation, such that infinity in the physical plane is mapped to the origin of the transformed domain. A lattice configuration conforming to a polar coordinate representation is then introduced, and the calculation in the far-field region is carried out using the transformed difference equations imposing the free-stream conditions at the origin. Sufficient overlap of this far-field lattice configuration, with the rectangular system, is maintained to obtain a proper patching of the two-flow domains.

‡ It would therefore be unwise to reduce the truncation error any more than is required to obtain results of meaningful accuracy.

§ Idiosyncrasies of finite difference procedures sometimes seem to be intolerant of seemingly simpler, more direct approaches.

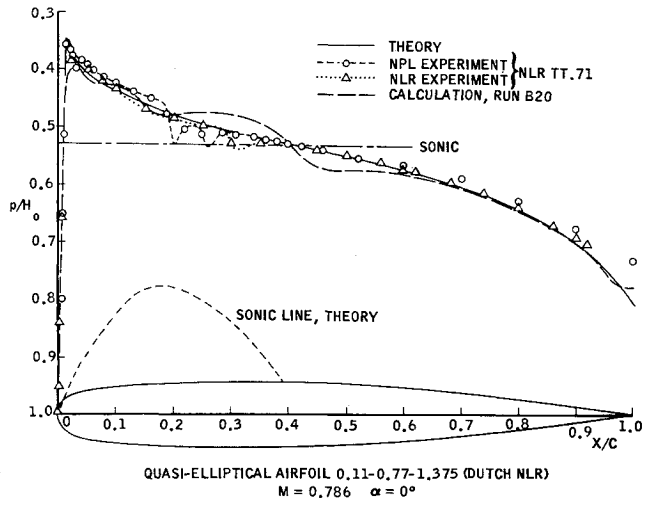

Fig. 3 Comparison of calculations with experiments for the shockless profile.

In the rectangular lattice region, a refinement of the lattice is also introduced where large flow gradients are expected; such as near the leading and trailing edges of the profile and at the expected location of shock waves. A fine mesh is embedded in the coarser mesh; such that the size of the coarser mesh is an integral multiple of the fine mesh. Suitable overlap of the two-lattice systems is again provided for proper matching of the two systems. In the overlap region adequate enhanced damping is incorporated to maintain stability, and the diffusive damping coefficients for the coarse and fine mesh systems are adjusted to maintain a viscosity match between the two systems.

In the marching process, the size of the time step is taken as a suitable fraction (less than one) times the allowable value as determined by a locally linearized stability analysis. The regions with a coarser space mesh are thereby permitted to march with a larger time step, with of course, a proper communication maintained between the two systems in the overlap region as the calculation progresses in the timewise direction.

The description of the finite difference method in the preceding paragraphs clearly does not cover all facets of the complex procedure, but sufficient details have been given to cover the essential aspects. With this procedure, we have calculated two supercritical examples, which we shall now describe in the next section.

IV Examples

The procedure as described in the previous section, has been programmed for the CDC 6400 computer, and the results for the two examples are presented in the present section. The first example selected was the symmetric NLR shockless profile No. 1 with the NLR designation, 0.11–0.75–1.375.[2] It has been derived by the hodograph method, yielding a shockless flow at a zero angle of attack and a Mach number of 0.786. This is one of the early examples calculated by Nieuwland and was the only profile for which the coordinates were available at the time our numerical calculations were planned. It, unfortunately, was a near singular profile in which the limiting line in the profile interior, in the nose region, was near the profile surface. This nearness caused a highly localized surface curvature peak which resulted in a near-cusped suction peak. The finite difference calculations were nevertheless carried out, as this example would be an exacting test for this procedure. The resulting pressure distribution is shown in Fig. 3 together with the hodograph results of Nieuwland. (Also shown here are the profile and some experimental results which we shall comment on shortly). The results of the finite difference method indicated that with the mesh spacing used (and this is indicated by the circle symbols), the truncation error was still sufficiently large in the pressure cusp region, so that the full suction peak could not be attained. The numerical results further shows an oscillatory pressure distribution downstream of the pressure peak, about the hodograph result, finally terminating in a weak-shock wave centered about the sonic point. This oscillatory discrepancy about the hodograph result can be directly attributed to the compression error introduced at the suction cusp by the local truncation error, reflecting back and forth between the sonic line and the airfoil surface, and resulting finally in a weak shock terminating the supersonic region.¶ This behavior perhaps should not be surprising, since it is just the behavior predicted by the Busemann-Guderley instability theory. Apart from the supersonic portion of the pressure distribution, the remaining subsonic portions, ahead of the cusp and downstream of the shock, agree remarkably well. Also shown in Fig. 3 are the experimental results for this profile obtained at the NLR (Amsterdam)[7] and NPL (Teddington).[7] The symbols denote the location of the pressure taps and the interpolation of the curves; especially the presence of shocks were those presented by the experimenters, who undoubtedly were guided by optical observations which were not given in the previously mentioned reference. The models were designed to take into account the boundary-layer displacement effects, though it is highly doubtful that the highly localized high-surface curvatures in the pressure cusp region could be faithfully reproduced in this manner.

For the second example we have computed the flow over a NACA 64A-410 profile at an angle of attack of 4° at a Mach number of 0.72. The resulting pressure distribution is shown in Fig. 4, where a comparison is made with the experimental results obtained by Stivers.[8] There is a good agreement on the lower side of the profile, but on the upper surface there is a discrepancy in the nose region and on the upstream and downstream sides of the shock. The discrepancies in the nose region and about the shock can be attributed to viscous effects, with the latter due definitely to the appearance of a lambda shock and a separation as the result of the boundary layer-shock wave interaction; in the leading edge region, the difference is probably due in part to an appearance of a short bubble separation, which prevents the flow from attaining the full leading edge expansion. (It may be recalled that in Stiver's tests the transition was natural with a Reynolds

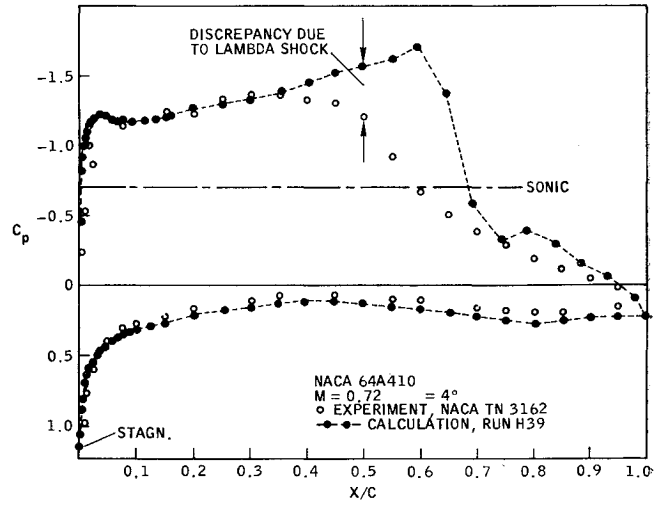

Fig. 4 Comparison of the calculation with experiments.

¶ Quite obviously the finite difference solution could be improved by eliminating the compression error, by taking a finer mesh in the region about the pressure cusp.

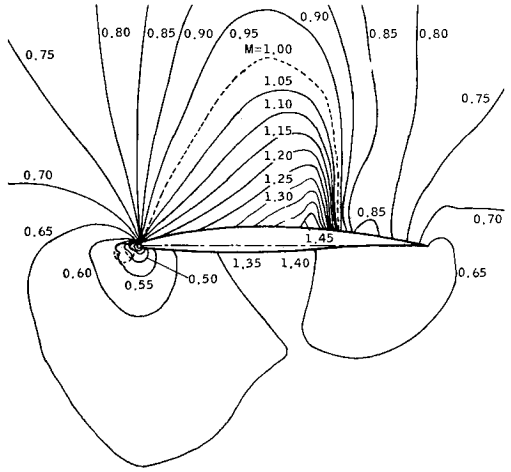

Fig. 5a Mach number contours for NACA64A4 10 airfoil at Mach 0.72 and $\alpha = 4°$.

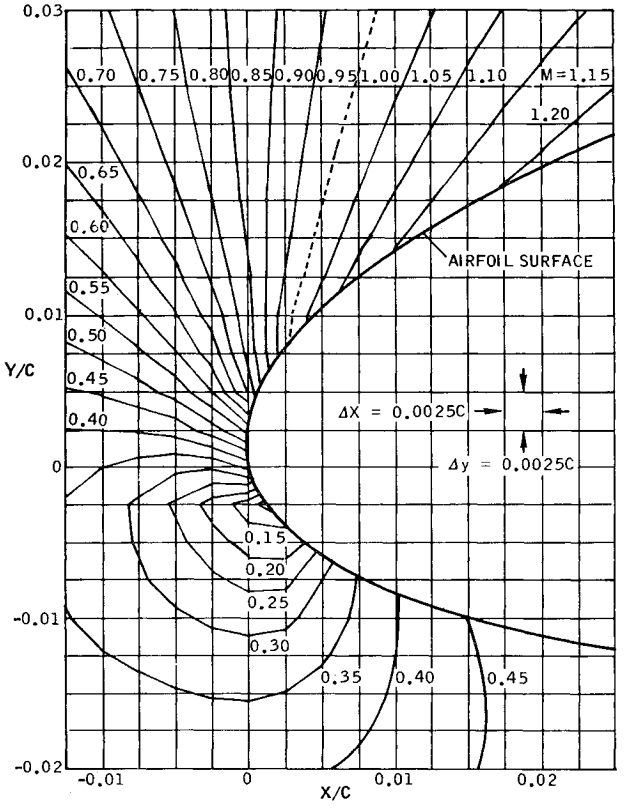

Fig. 5b Details of Mach contours in region covering first 2.5% of chord; NACA 64A410 airfoil, Mach 0.72, $\alpha = 4°$.

number based on a six-in. chord of approximately 10^6). In Figs. 5a and 5b, the resulting constant Mach number lines are next plotted, with the latter figure illustrating the nature of the detail which we have required in the nose region. The latter plot has been obtained by an automatic plotter, where for simplicity straight lines instead of parabolic arcs have been used to connect the interpolated points obtained essentially by a linear interpolation of the computed values. In Fig. 5a there are a number of irregularities in the isobars as noted by the encirclement, and these must be attributed to truncation errors. The probable configuration of the isobars that might result by a refinement of the mesh in these regions is indicated by the dashed lines. The additional effort required to remove the local irregularities was felt to be unwarranted, since we were primarily interested in the pressure distribution on the airfoil, which should not be affected significantly by these irregularities. Finally in Fig. 6 we

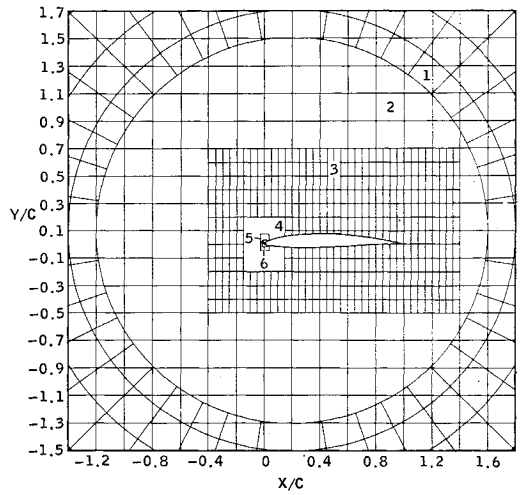

Fig. 6 Mesh systems utilized in calculating flow about 64A410 airfoil.

show the system of lattice points used in the aforementioned calculations. In total, there are approximately 3700 points with 53 points taken on the upper side of the profile. The mesh dimensions in the various regions are shown in Table 1.

Calculations required approximately 3.5 hr on the CDC 6400 computer to obtain a meaningful result. For this initial example the primary effort was directed not only towards obtaining a result, but to understand the detailed evolution of the flow, with no attempt made to obtain economical results. This large expenditure of time is directly attributable to the large number of mesh points used, which may in fact be more than is required, to the slowness of the convergence to a steady state, and finally to the numerous printouts of the intermediate results for diagnostic purposes. Quite clearly there is much that can be done to decrease the computing time, and we plan to direct our efforts in the future toward this goal.

V Final Remarks

The few examples presented here indicate that the present numerical method can yield promising results, and with further experience it can be developed into a reliable practical procedure to calculate supercritical inviscid flows of accuracies of engineering value.

Whether one should label the present procedure as an exact procedure is rather a moot question, since it is not only impossible to take the limit, in practice, to a vanishing small mesh spacing, but it is seldom possible from a financial standpoint or due to computer incapacity even to determine the consequences of a smaller mesh for a problem of the complexity as the present one. Setting aside these limitations, one has still the question of whether in principle, the calculations remain stable as the mesh is decreased indefinitely, since the primary source of the stability in problems such

Table 1 Mesh dimensions

Region 1	9 Rings $\sim R = 1.4C \times 8/N, N = 0,8$	
	40 Rays $\sim \Delta\theta = 9°$	
Region 2	$\Delta X = 0.20C$	$-1.4C \leq X \leq 1.8C$
	$\Delta Y = 0.20C$	$-1.5C \leq Y \leq 1.7C$
Region 3	$\Delta X = 0.05C$	$-0.4C \leq X \leq 1.4C$
	$\Delta Y = 0.10C$	$-0.5C \leq Y \leq 0.7C$
Region 4	$\Delta X = 0.0125C$	$-0.15C \leq X \leq 0.15C$
	$\Delta Y = 0.025C$	$-0.20C \leq Y \leq 0.20C$
Region 5	$\Delta X = 0.0025C$	$-0.025C \leq X \leq 0.0375C$
	$\Delta Y = 0.005C$	$-0.050C \leq Y \leq 0.030C$
Region 6	$\Delta X = 0.0025C$	$-0.0125C \leq X \leq 0.025C$
	$\Delta Y = 0.0025C$	$-0.020C \leq Y \leq 0.030C$

as our present one is just those truncation errors which are gradually being eliminated. These difficulties raise a crucial question, which concerns all numerical solutions of complex problems; namely, how good are the resulting numerical solutions? Where exact-analytical solutions or pertinent experimental results are on hand, the previous question can be readily answered. In our present problem we have on hand the shockless supercritical hodograph solutions calculated by Nieuwland, and will shortly have two-dimensional, high Reynolds number tests by Rainbird for the NACA 64A-410 airfoil, which will serve for comparison purposes. Although the calculation for the Nieuwland profile requires further refinement, and a high Reynolds number comparison test is yet to be obtained for the NACA 64A-410 profile, we hope that the present results will serve to demonstrate the potential of the present unsteady finite difference procedure.

With regard to our future efforts, we plan to implement as rapidly as possible, several modifications to decrease the computer time by decreasing both the number of points required and the subsidence time to attain a steady state. With an economical procedure on hand, there is a plethora of cases which one would like to compute, including flows at a Mach number of 1 and at low-supersonic Mach numbers, as well as axial-symmetric cases, which may be obtained by a trivial extension of the present planar procedure.

References

[1] Lax, P., "Weak Solutions of Nonlinear Hyperbolic Equations and Their Numerical Computation," *Communications on Pure and Applied Mathematics*, Vol. VII, 1954, pp. 159–193.

[2] Nieuwland, G. Y., "Transonic Potential Flow Around a Family of Quasi-Elliptical Aerofoil Sections," TR. T. 172, 1967, National Aerospace Laboratory, Amsterdam, Netherlands.

[3] Busemann, A., "The Drag Problem at High Subsonic Speeds," *Journal of Aeronautical Sciences*, Vol. 16, 1949, pp. 337–344; also Guderley, G., "Shocks in Subsonic-Supersonic Flow Patterns," *Advances in Applied Mechanics*, Vol. III, Academic Press, New York, 1953.

[4] Morawetz, C., "On the Non-Existence of Continuous Transonic Flows Past Profiles," *Communications on Pure and Applied Mathematics*, Vols. 9 and 10, 1956–1957.

[5] Frankl, F. I., "On the Formation of Shocks in Subsonic Flows With Local Supersonic Velocities," TM No. 1251, 1950, NACA.

[6] Hirt, C. W., "Heuristic Stability Theory for Finite Difference Equations," *Journal of Computational Physics*, Vol. 2, No. 4, June 1968, pp. 335–355.

[7] Spee, B. M. and Uijlenhoet, R., "Experimenteel Onderzoek aan Symmetrische Quasi-Elliptische Profielen," Interim Report TT.71, 1967, National Aerospace Laboratory, Amsterdam, Netherlands.

[8] Stivers, L., "Effects of Subsonic Mach Number on the Forces and Pressure Distribution of Four NACA 64A-Series Airfoil Sections," TN 3162, 1954, NACA.

DECEMBER 1970 AIAA JOURNAL VOL. 8, NO. 12

Wall-Wake: Flow behind a Leading Edge Obstacle

PASQUALE M. SFORZA* AND ROBERT F. MONS†
Polytechnic Institute of Brooklyn Long Island Graduate Center, Farmingdale, N. Y.

An investigation of the three-dimensional, incompressible wake behind a blunt obstacle located at the leading edge of a flat plate is presented. Configurations studied included the "clean" flat plate, and the flat plate with a rectangular, a square, or a two-dimensional obstacle fitted to the leading edge of the plate. Experimental results compare well to a mathematical model based on the Oseen linearization for wake-like diffusive flows. Based on mean flow measurements, transition to turbulence was encountered for all the configurations examined. Such wakes are characterized by a region of strong vorticity immediately behind the obstacle followed by a region of turbulent diffusion. Bulk properties of the wakelike flow and the applicability of the theoretical model were found to be highly dependent on the geometry of the obstacle.

Nomenclature

c_f = $\tau_w/\frac{1}{2}\rho U_\infty^2$, local skin-friction coefficient
d = obstacle height
e = d/L, inverse fineness ratio
L = length of obstacle
$u, \Delta U$ = $(U_\infty - U)$, mean velocity perturbation
U = local mean velocity
U_τ = $U_\infty(c_f/2)^{1/2}$, shearing velocity
x,y,z = streamwise, normal, and transverse coordinates
X = transformed streamwise coordinate, Eq. (4)
δ^* = displacement thickness
ϵ = eddy viscosity parameter, Eq. (3)
ν = kinematic viscosity

Subscripts

b = denotes basic two-dimensional boundary-layer flow
max = denotes maximum conditions
w = denotes wall conditions
$\frac{1}{2}$ = denotes conditions at a station where $u = u_{\max}/2$
∞ = denotes freestream conditions

Superscript

$(\bar{\ })$ = denotes $(\ )/d$

Presented as Paper 69-747 at the CASI/AIAA Subsonic Aero- and Hydro-Dynamics Meeting, Ottawa Canada, July 2–3, 1969; submitted Aug., 14, 1969; revision received May 6, 1970. This research was supported by the Air Force Office of Scientific Research under Contract AF 49(638)-1623, Project 9781-01.

* Associate Professor of Aerospace Engineering. Member AIAA.

† Research Associate.

I. Introduction

THE occurrence of wakes behind obstacles on flat plates, which, for the purpose of this report, shall be called "wall wakes," is quite frequent. Protruberances on bodies in a moving stream, interfacial vehicles such as trains or cars, and land structures in a wind are just a few examples of configurations that can produce wall wakes. Furthermore, nontangential injection of a gas or liquid through a wall into a stream passing over the wall will produce a flow which